The observed Trojans and the global dynamics around the Lagrangian points of the Sun–Jupiter system.

Philippe Robutel[*], Frederic Gabern[†] and Àngel Jorba[†]

Abstract

In this paper, we make a systematic study of the global dynamical structure of the Sun–Jupiter L_4 tadpole region. The results are based on long-time simulations of the Trojans in the Sun, Jupiter, Saturn system and on the frequency analysis of these orbits. We give some initial results in the description of the resonant structure that guides the long-term dynamics of this region. Moreover, we are able to connect this global view of the phase space with the observed Trojans and identify resonances in which some of the real bodies are located.

Keywords: Frequency analysis, Trojan asteroids, resonances, Arnold web.

Contents

1 Introduction **2**

2 Frequency Map and global structure of the phase space **2**

3 Analysis of the observed Trojans **9**

4 Conclusions **13**

References **14**

[1]Astronomie et Systèmes Dynamiques, IMCCE-Observatoire de Paris, 77 Av. Denfert-Rochereau, 75014 Paris, France. e-mail: `robutel@imcce.fr`

[2]Departament de Matemàtica Aplicada i Anàlisi, Universitat de Barcelona, Gran Via 585, 08007 Barcelona, Spain. e-mails: `gabern@mat.ub.es, angel@maia.ub.es`

1 Introduction

The long-term stability of the Jovian Trojan asteroids is a classical problem of dynamical astronomy. In the literature, this question is usually approached using analytical (see [11], [4], [12], [29], [8]) or numerical methods. Among the numerical studies, two points of view are prominent:

(1) *Local approach*: Definition and computation of proper elements and proper frequencies. A synthetic theory for the proper elements was first established by Milani [20, 21]. Later on, Beaugé and Roig developed a semi-analytical theory for Trojan proper elements [1]. The question of Trojan proper frequencies was also tackled by [10].

(2) *Global approach.* Since the work by [17], where the spatial distribution of the escape times was studied, different attempts to describe the global dynamics of the co-orbital region have been done: [19], [24] and [30].

In this paper, we try to combine these two different approaches by placing several hundreds of observed Trojans in the corresponding global dynamical background.

First, we show some initial results of a global and systematic study of the tadpole region near the Jupiter co-orbital L_4 point [26]. We describe some of the families of resonances that are fundamental to understand the complicated structure underlying the 1:1 mean motion resonance between Jupiter and a Trojan. The computations are based on the Frequency Map analysis [15] and the results rely on an estimate of the chaoticity of some relevant slices of the phase space. These global pictures of the dynamical structure around the L_4 co-orbital region and the knowledge of the specific values of the fundamental frequencies allow us to identify the resonances that arrange the main structures of the phase space.

Once these global dynamical pictures are obtained, a natural question is what information they provide concerning the real Trojan asteroids. In this regard, we explain a way of superimposing the observed Trojans in these dynamical maps and we are able to identify actual asteroids inside some of the main resonances of the global pictures.

The simulations are based on a direct numerical integration of the Restricted Four-Body Problem defined by Sun, Jupiter, Saturn and the asteroid (SJS model). [10] already showed that for studying the Trojan problem, restricted three-body models are not enough. Moreover, in [7], some relatively simple semi-analytic four and five body models (3-body models with 2-dimensional quasi-periodic forcing [9]) were used to study this problem and also proved not accurate enough for the complete description of the fundamental frequencies of the Trojan asteroids. Thus, more planetary frequencies have to be taken into account.

In [26], it is shown that the SJS model already captures the main global dynamical structures of the co-orbital regions. Actually, the addition of Uranus and Neptune to the problem, does not affect the main features of the phase space, but just shifts slightly the location of the resonances and makes everything a little bit more unstable [26].

2 Frequency Map and global structure of the phase space

In Figure 1, we show a dynamical map of the tadpole region of the leading Lagrangian point L_4 (similar pictures are obtained in the L_5 case). This picture is generated by an integration of 32,000 fictitious Trojans. Their initial semi-major axis and eccentricities are chosen on a grid of 400×80 points belonging to the domain

$$(a, e) \in \mathcal{A} = [5.2035, 5.4030] \times [0.05, 0.30], \tag{1}$$

Planet freq. ("/yr)		Asteroid freq.	Min. ("/yr)	Max. ("/yr)
n_5	109254.63165	ν	7000	9500
n_6	43995.34975	g	250	450
g_5	4.02760	s	-50	10
g_6	28.00657			
s_6	-26.03912			

Table 1: Fundamental frequencies. The first two columns show the fixed frequencies used for the planets; subscript 5 stands for Jupiter and 6 for Saturn. In the last three columns, we show the minimum and maximum values (for the initial conditions considered) of the frequencies of the test-particles.

where the points in the mesh are equally separated at a distance of $\Delta a = 0.0005AU$, for the a axis, and $\Delta e = 0.003125$, for the e axis. The remaining initial elliptic elements are fixed and equal the following values: $\sigma = \lambda - \lambda_5 - \pi/3$, $\sigma_g = \varpi - \varpi_5 - \pi/3$, $\Omega = \Omega_5$ and $I = I_5 + 2°$, where the subscript 5 denotes the elements of Jupiter. The choice of these values is natural if one realizes that, for the Sun–Jupiter Elliptic Restricted Three Body Problem (ERTBP), the elliptic elements of the L_4 point are: $a = a_5$, $e = e_5$, $\sigma = \sigma_g = 0$, $\Omega = \Omega_5$ and $I = I_5$.

The trajectories of these bodies are numerically integrated using a symplectic integrator of the family $SABA_n$ [16] on two consecutive time spans of $5My$ each. Then, using the Frequency Map Analysis method [14, 15], two determinations of their fundamental frequencies are associated to every Trojan (one for each time span).

If we assume that the motion of Jupiter and Saturn is quasi-periodic (which is a very natural assumption on the $10My$ considered here [14, 27]) the orbit of this planetary system lies on a 5-dimensional invariant torus, with fundamental frequencies $(n_5, n_6, g_5, g_6, s_6)$. The two first frequencies are the proper mean motions (frequencies associated to the orbital motion) of Jupiter and Saturn, respectively; while the other three are the secular frequencies of the Sun–Jupiter–Saturn system (see Table 1).

In these conditions, the motion of the asteroid can be seen as a 3-degrees of freedom Hamiltonian system with quasi-periodic forcing. This implies that a quasi-periodic trajectory is parametrized by eight fundamental frequencies. Five correspond to the quasi-periodic forcing and the remaining three characterize the dynamics of the Trojan [13]. These three fundamental frequencies (ν, g, s) are respectively the proper libration frequency (connected to the libration in the 1:1 Mean Motion Resonance (MMR) with Jupiter), the proper precession perihelion frequency of the asteroid and the one corresponding to its node. They are the image of the Frequency Map, which can be defined as [15]

$$F_{\theta_0} : (a, e, I) \longrightarrow (\nu, g, s), \tag{2}$$

where $\theta_0 = (\lambda_0, \varpi_0, \Omega_0)$ is the fixed phase vector given above.

In general, the Frequency Map is a correspondence from an action space to a frequency space [15]. Even though this is not exactly the case here, our choice of initial phases θ_0 makes the elements (a, e, I) very close to action variables [26]. Thus, we can assume that, at least inside regular regions of the phase space, the map F_{θ_0} defines a one–to–one correspondence between the domain $\mathcal{D} = \mathcal{A} \times \mathcal{S}$ (where A is given by (1) and $\mathcal{S} = I_5 + [0°, 38°]$ is the interval of inclinations considered) and its image $\mathcal{F} = F_{\theta_0}(\mathcal{D})$. The last three columns of Table 1 give the extremes

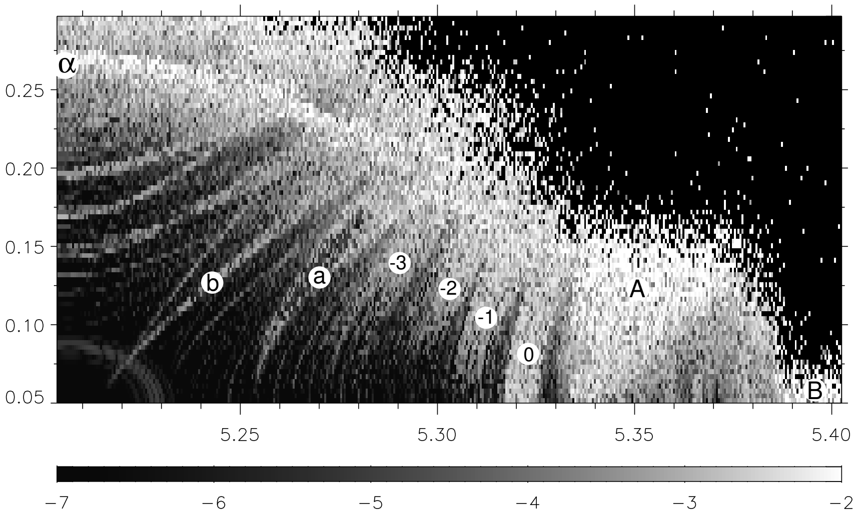

Figure 1: Dynamical map of the tadpole region surrounding L_4. It corresponds to a section of the phase space in the plane (a_0, e_0) where the other initial elliptic elements are fixed (for instance, the inclination is $I = I_5 + 2°$). The gray code corresponds to the temporal variation of ν in logarithmic scale: $\log \delta\nu$ (units: My^{-1}). The symbols inside the plot indicate main resonant structures. See text for more details.

of this frequency domain $\mathcal{F}$. For theoretical reasons discussed in [26], the frequency set $\mathcal{F}$ is a representative domain in the sense that the fundamental frequencies of a given Trojan belong to $\mathcal{F}$, no matter which their initial phases are. This assumption is satisfied for the large majority of the observed Trojans.

Therefore, the determination of the fundamental frequencies ν, g and s is the key point of our study. Besides giving an estimation of the diffusion rate used to detect instabilities [14, 28], it allows us to study the dynamical structures of the frequency space. Indeed, it is in this space (see Figure 2) that phenomena associated to resonances become clear and are quite easy to identify [26]. In addition, the fundamental frequencies are considered in Section 3 as proper elements [20], and are used to locate observed Trojans on our dynamical maps (i.e. Figure 1).

The bodies remaining inside the co-orbital region during the whole integration (10 My) are colored, in Figure 1, according to the relative variation of the proper libration frequency $\delta\nu = (\nu_1 - \nu_2)/\nu_1$. Being ν_1 (ν_2) the determination of the proper libration frequency, ν, on the 1st (2nd) time-interval. The color code goes from dark gray, corresponding to motion close to quasi-periodic ($\delta\nu < 10^{-7}$), to light gray, for strongly irregular motion ($\delta\nu > 10^{-2}$). The black points (i.e., the top-right corner of the plot) correspond to initial conditions that escape from the co-orbital region before the 10 My integration ends.

Given this color code, it is clear from Figure 1 that the instability increases with the distance from the L_4 equilibrium point (placed in the left-bottom corner in this coordinates), ending in the black region (near the top-right corner). This leads to split this part of the phase space into three different domains: the escape domain (black), the high diffusion domain, defined arbitrarily by $\delta\nu > 10^{-3}$ (light gray to white), and the long-term stability domain, with $\delta\nu < 10^{-4,5}$ (dark gray).

By comparing this figure (and also Figure 3) with the ones obtained by [30], we note that a strong correlation exists between the value of $\delta\nu$ and the escape time from the co-orbital regions. More precisely, our high diffusion domain ($\delta\nu > 10^{-3}$) corresponds to an escape time of about 10^7–10^8 years, while the escape time inside the long-term stability region is larger than 10^9 years.

These two domains are strongly interpenetrate. Indeed, Figure 1 shows a kind of Arnold web made of unstable tongues (light gray) generated by resonances. These structures are practically isolated at a small distance of L_4 and they have a trend to overlap when the distance increases, until complete overlapping is reached close to the border of the black area. Each one of these tongues is generated by resonances that can be split in four different families.

Family 1 The first two families belong to a larger class of resonances, which is the one that gathers the secondary resonances between the proper libration frequency ν and a linear combination of planetary mean motions. The first family involves the high frequency n_5, while the second family is related to the short period combination $n_5 - 2n_6$. Although this distinction in two different sets is quite arbitrary, it becomes natural if one realizes that the resonances related to n_5 already arise in the ERTBP (or even in the circular one), while, of course, the second family of resonances only can appear when the perturbation of two planets is considered.

Indeed, in the case of the RTBP (circular and planar cases) the secondary resonances associated to n_5 take the form:

$$p\nu - n_5 + g = 0\,,\ \text{with } p \in \{12, 13, 14\}. \tag{3}$$

Since $g \ll \nu \ll n_5$ (see Table 1), the resonances (3) are isolated and do not generate significant chaotic behaviors. On the contrary, as soon as a non zero eccentricity is given to Jupiter, the resonance (3) has to be replaced by the multiplet

$$p\nu - n_5 + qg = 0\,,\quad \text{where } q \text{ is an integer}, \tag{4}$$

that generates, by overlapping, a large chaotic zone. It is worth to mention that this kind of secondary resonances can be seen as the overlapping of the 1:1 MMR with the high order resonances (p:p$\pm$1). By overlapping, these narrow resonances that accumulate far before reaching the stable an unstable L_3 manifolds (surfaces that separate tadpole orbits from horseshoe orbits, [25]), generate strong global instability.

The number of harmonics associated to the first family of resonances still increases when Saturn's perturbation is taken into account. Indeed, because of the additional secular frequencies of the planetary system g_5, g_6 and eventually s_6, the resonant relation defining the first family becomes:

$$p\nu - n_5 + qg + q_5 g_5 + q_6 g_6 = 0\,,\quad \text{with } q + q_5 + q_6 = 1. \tag{5}$$

Two of the most important contributions of this family are visible in Figure 1. The large gap above the white region indicated by "B" is generated by (5) with $p = 14$, while the V-shaped (large light gray to white) region labeled by "A" is associated to $p = 13$.

Family 2 The second family in the class of secondary resonances, that we will call *secondary three body resonance*, plays an important role in the Trojan swarms. This type of resonance appears when the libration frequency ν and the high frequency $n_5 - 2n_6$ are close to commensurability. Among all the possible combinations, the ones that generate large chaotic regions are given by:

$$5\nu - 2(n_5 - 2n_6) + pg + p_5 g_5 + p_6 g_6 = 0\,, \quad \text{with } p + p_5 + p_6 = -2. \tag{6}$$

[24] first mentioned the possibility of instabilities generated by this family.

In the same way as in *Family 1*, because the secular frequency g is more than fifteen times larger than g_5 and g_6, a given p defines a multiplet of resonant harmonics. The four widest regions associated to this family are indicated in Figure 1 by the numbers 0 to -3 corresponding to the value of the integer p. It is important to mention that these resonances do not come from the direct action of Saturn, but from the short period perturbations of Jupiter's orbit due to Saturn (the same type of effect appears in [6] for a different problem).

Indeed, the frequencies corresponding to $n_5 - 2n_6$ and to the Great Inequality $2n_5 - 5n_6$ are associated with terms of large amplitude in the quasi-periodic approximation of Jupiter's eccentricity. For small Trojan eccentricity, resonant regions corresponding to different members of this family are isolated between them. But for larger Trojan eccentricities, these regions overlap in the neighborhood of the long white half-arch labeled by "α".

Family 3 This white arch (that cuts the vertical axis at about $e = 0.265$) corresponds to the location of the secular resonance $s = s_6$. This resonance, which influence on the Trojans was already suggested by [31] and studied by [2], [20], [5] and [18] (among others) is known to induce very strong instabilities in the neighborhood of the long-term stability domain. Indeed, the majority of the Trojans that enter this secular resonance escape the co-orbital region in a few tenths of million years. Apart from this first order resonance, a lot of other secular resonances are present in the Trojan phase space, especially of the form:

$$qs + q_6 s_6 + p_5 g_5 + p_6 g_6 = 0, \tag{7}$$

with $q + q_6 + p_5 + p_6 = 0$ and $(q + q_6)$ even.

The significance of the secular resonances increase with the initial inclination of the Trojan, but even for high inclinations, these resonances are thin and isolated [26]. For instance, the little quarter of circle in the left bottom of Figure 1, where the diffusion rate is of about 10^{-5}, corresponds to the location of the sixth order secular resonance $2s - 3g_5 + g_6 = 0$.

Family 4 The two most representative members of the last family are associated to the unstable structures denoted by "a" and "b" in Figure 1. They penetrate deeply inside the long-term stability region. These structures, and the other thin curves in the left side of "b", are generated by the Great Inequality. From the "frequencies point of view", this phenomenon leads, inside the resonance, to the relations:

$$4g + (2n_5 - 5n_6) + q_5 g_5 + q_6 g_6 + r_6 s_6 = 0\,, \text{ with } q_5 + q_6 + r_6 = -1. \tag{8}$$

Contrarily to what happens in *Family 1* and *Family 2*, the relation (8) does not contain the libration frequency ν and, thus, it is not a secondary resonance of the usual type. Although these structures seem to be very narrow and isolated, they play an important role in the slow diffusion process that drives Trojans from the long time stability inner regions to the short time stability boundary. An example of this transport along resonances is shown in Figure 2 and discussed below.

The interest of this family (and to a less extend of *Family 2*) is enhanced by the fact that some observed Trojans seem to evolve inside these resonances (see Section 3) and, consequently, may be subject to long-term transport phenomena.

In order to illustrate that it is in the frequency space where the dynamical phenomena associated to resonances can be easily interpreted, we show in Figure 2 the projection on the (g, s) plane of the image of $\mathcal{A} \times (I_5 + 2°)$ by the Frequency Map F_{θ_0}. This plot is the counterpart of Figure 1 in terms of frequencies.

Figure 2 is made up of a union of curves (more or less smooth) that are the image of the lines $e_0 =$ constant by the Frequency Map. The triangular shape of the picture is explained in the following way: the upper vertex of the triangle corresponds to the L_4 point, and the right and left edges correspond, respectively, to the line $e = 0.05$ (eccentricities lower limit) and to $a = 5.2035$ AU (semi-major axis lower bound). These curves are smooth in regular regions, but singularities arise in chaotic zones. Singularities of the Frequency Map are directly correlated with instabilities of the corresponding trajectories (see [15] for more details).

The resonances of *Family 3* and *Family 4* are very easy to identify in this plot. The vertical lines, where frequencies accumulate near $g =$ constant, correspond to *Family 4*. In particular, the straight lines marked as "a" and "b" (these resonances are also shown in Figure 1 with the same labels) belong to *Family 4* and clearly are of the form $g =$ constant. Horizontal lines correspond to *Family 3* and are of the type $s =$ constant. In particular, the important resonance $s = s_6$ (seen in Figure 1 as an arch denoted by α) is easily identified in the central part of the picture. Note that above this horizontal line the dynamics is more regular than below of it, where the chaotic and escaping dynamics prevails.

In Figure 2, straight lines with finite (and different from zero) slope also appear. They correspond to resonances of the type $pg + qs + 2n_5 - 5n_6 + p_5 g_5 + p_6 g_6 + q_6 s_6 = 0$ with $p + q + p_5 + p_6 + q_6 = 3$ and $q + q_6$ even. These resonances are not discussed in this paper (see [26] for more information).

Of course, resonances belonging to *Family 1* and *Family 2* do not appear in Figure 2 as clearly as the secular ones. Indeed, to identify these resonances, one needs to look at the projection on the (ν, g) plane. Nevertheless, these secondary resonances appear in Figure 2 as singularities of the Frequency Map and we have marked them with the same labels as in Figure 1: "A", "B", "0", "-1", "-2" and "-3".

In order to illustrate the influence of *Family 4* on the long-term transport from the inner libration region to the outer unstable zone, we have performed an integration of a fictitious body with an initial condition satisfying the $4g + (2n_5 - 5n_6) - g_5 = 0$ resonance relation (label "a" in Figures 1 and 2). This particle follows a path along this resonance (downward in Figure 2), crosses the secular resonance $s = s_6$ and, finally, escapes the co-orbital region. This path in the frequency space is generated by computing the fundamental frequencies of the body for every consecutive interval of 5 My and superimposing them (using thick black points) on Figure 2. This allows to follow its long-term diffusion in the frequency space. During the first 215 My, the fictitious Trojan stays inside the resonance "a" with the secular frequency s evolving in the range $[-19, -16.72]$ ("/y) without a well-defined trend. Then, the trajectory leaves the resonance "a" and wanders around it for the next 100 My (crossing the resonance several times). Meanwhile, the frequency s decreases from -19 "/y to -23.5 "/y. Finally the path crosses downward the $s = s_6$ horizontal line and the fictitious Trojan enters the large chaotic zone associated to this resonance, where it remains from the 315 to the 355 My of integration time, before being ejected. Other examples of diffusion along resonances and connections between them are presented in

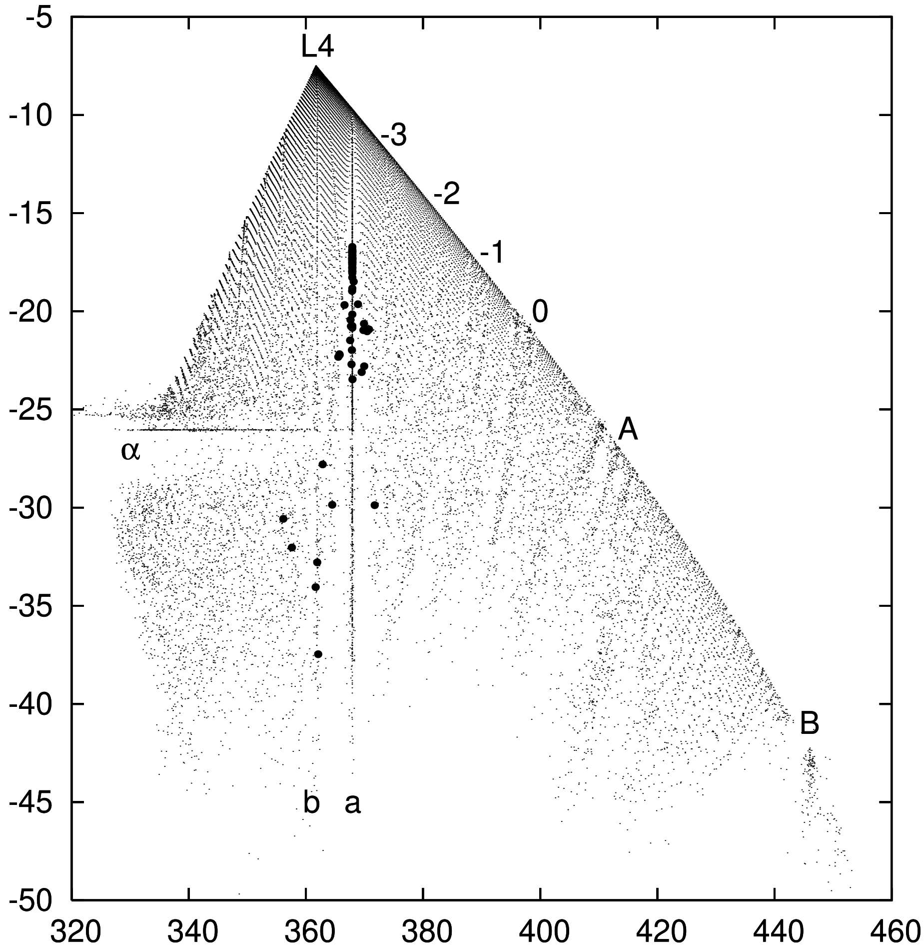

Figure 2: Projection on the (g, s) plane (units: "/yr) of the image of $(a, e, I) \in \mathcal{A} \times (I_5 + 2°)$ by the Frequency Map (2). It is in this space where resonances of the third and fourth family are easy to identify. The labels indicate the same resonant structures shown in Figure 1. The thick black points correspond to a path of a fictitious body that, starting in the resonance "a" (near $s \approx -17$), is subject to long-term transport along this resonance. This body is ejected from the co-orbital region after 355 My of integration time. See text for more details.

[26], showing the implication of the resonant structure in the long-term dynamics of the Trojan asteroids.

The dynamical role of the four families of resonances presented above depends on the value of the initial inclination. This is particularly true for *Family 3* and *Family 4*. As we will see in Figure 3, when the inclination is small, *Family 3* resonances seem to be negligible, except for the important case $s - s_6 = 0$. Then, as the inclination becomes larger, new secular resonances appear. At $I \sim 12°$, a small unstable region around L_4 marks the birth of the resonance $3s - s_6 - 2g_5 = 0$. Similarly, other secular resonances appear for $I \sim 16°$, while the latter ones move farther from the Lagrangian point. On the contrary, the influence of *Family 4* decreases when the inclination, I, is increased. The dynamical implications of this phenomena are discussed in [26].

3 Analysis of the observed Trojans

Once the global structure is known, it is tempting to locate the observed Trojans in our dynamical maps (in plots similar to Figure 1). In this regard, we downloaded from [3] their osculating elliptic elements at the Julian date 2452200.5 (October 10th, 2001) to be used as initial conditions for the simulations.

Unfortunately, a direct projection of these initial conditions into the dynamical maps would be meaningless. This is true even if we project in Figure 1 (where recall that $I = I_5 + 2°$) only the Trojans with small initial inclination [30].

Indeed, since the initial phases of a given asteroid are, in general, different from θ_0 (the ones that define the Frequency Map (2)), a direct projection would locate the Trojan at the wrong place (because the global dynamical background would be different from the actual one). Although this procedure works rather well when the goal is to locate a body on a low resolution map [30], it fails when we ask for an accurate position of the asteroid, which is precisely what we need to connect the real Trojans to the narrow dynamical structures like the resonant families defined in Section 2.

To get rid of this "phase inconvenient", what we do is to look at the frequency space $\mathcal{F}$. For every observed Trojan j with initial conditions (a_j, e_j, I_j) and $\theta_j = (\lambda_j, \varpi_j, \Omega_j)$, we compute its basic frequencies $(\nu_j, g_j, s_j) = F_{\theta_j}(a_j, e_j, I_j)$, in the same way as it was done for fictitious particles in Section 2. As $F_{\theta_j}(a_j, e_j, I_j)$ belongs to $\mathcal{F}$, the quantities that we are looking for are given by:

$$(\tilde{a}_j, \tilde{e}_j, \tilde{I}_j) = F_{\theta_0}^{-1} \circ F_{\theta_j}(a_j, e_j, I_j). \tag{9}$$

This expression is well defined when the Hamiltonian system governing the motion of the Trojans is integrable. Two trajectories having respectively $(\tilde{a}_j, \tilde{e}_j, \tilde{I}_j, \theta_0)$ and $(a_j, e_j, I_j, \theta_j)$ as initial conditions are generally not the same, but they lie on the same invariant torus and, therefore, are dynamically equivalent. Thus, our choice (9) is natural in the sense that a frequency vector is not equivalent to a trajectory but to an invariant torus.

In practice, two main difficulties have to be overcome. The first one comes from the fact that our Hamiltonian is not integrable on an open subset of the phase space, even though it is integrable on the Cantor set of invariant tori (this makes F_{θ_0} well defined on this Cantor set). In particular, the frequency map F_{θ_0} has singularities (aseptically in the neighborhood of the resonances), and, thus, F_{θ_0} is probably not invertible. The second is that only a finite number of points of $\mathcal{F}$ is known: The domain of initial conditions $\mathcal{D}$ is sliced in 20 planes (a, e) for fixed inclinations $I - I_5 \in \tilde{\mathcal{S}} = \{0°, 2°, 4°, \ldots, 38°\}$. For each of these planes, we consider 32,000

Cat. num.	Name	p	q	q_5	q_6	dist. ("/yr)
1749	Telamon	13	-12	3	10	2.42080e-02
5259	Epeigeus	13	-12	6	7	2.26021e-02
20739	1999XM193	13	-13	4	10	4.05032e-03

Table 2: Family 1. Actual Trojans at a distance smaller than 0.1"/yr of the resonance $p\nu - n_5 + qg + q_5g_5 + q_6g_6 = 0$.

initial conditions (see Section 2). Thus, $\mathcal{D}$ is replaced by the discrete set $\tilde{\mathcal{D}}$ containing 640,000 points. The discrete frequency space $\tilde{\mathcal{F}} = F_{\theta_0}(\tilde{\mathcal{D}})$ contains less than 420,000 points, because an important fraction of initial conditions of $\tilde{\mathcal{D}}$ correspond to escaping or very chaotic trajectories, for which the quasi-periodic approximation is meaningless. Then, for a given actual Trojan, we can approximate the elements $(\tilde{a}_j, \tilde{e}_j, \tilde{I}_j)$, defined in (9), by the quantities (a_j^*, e_j^*, I^*) such that the expression

$$d_{j,0} = \left\| F_{\theta_j}(a_j, e_j, I_j) - F_{\theta_0}(a^*, e^*, I^*) \right\|_2 \tag{10}$$

is minimal in the grid $\tilde{\mathcal{D}}$ ($\|\cdot\|_2$ denotes the euclidean norm in $\mathbb{R}^3$).

In Figure 3, we plot these "reference elements" (a_j^*, e_j^*), corresponding to the observed L_4 and L_5 Trojans for which the euclidean norm described above is smaller than 1 "/yr, on the global dynamical maps around the L_4 point (this is justified by the fact that no significant differences are found between the dynamical structures of the L_4 and L_5 tadpole regions). Only the first 10 of the 20 dynamical maps considered are shown.

These pictures show that the majority of the Trojans are inside the long-time stability region (this was already noticed by many authors: [19], [24] and [30], for instance) and also suggest that some actual Trojans may stay inside (or very close to) some of the resonances described in Section 2. This is rather easy to check when one has the basic frequencies of the observed asteroid.

In Table 2, we show the actual Trojans that, for the SJS system, lie very close (at a distance smaller than 0.1 "/yr) to some resonance corresponding to *Family 1* (5), up to order 40. The first and second columns display the catalog number and the name of the particular asteroid. In the last column of the table, we give the distance to the exact resonance in "/yr. The remaining columns are devoted to the multiplet that defines the particular resonance inside the family.

In Table 3, we show the Trojans that, up to order 16, are at a distance smaller than 0.1 "/yr of some resonance corresponding to *Family 2* (6). The last column shows the inclination in which the corresponding asteroid is found in Figure 1 (blank means that the asteroid is at a distance larger that 1 "/yr of any of our dynamical maps and, thus, it is not drawn).

In Table 4, we show some of the real Trojans that are at a distance smaller than 0.1 "/yr of some representative secular resonance of *Family 3* (7). The computations are done up to order 14, and only 10 of the 46 actual cases found are shown. Note that some Trojans (i.e. 7119-Hiera) may even be very close to a double resonance. Double resonances were already suggested as a possible explanation for the "stable chaos" of some asteroids found in [20] and mentioned by [5], for high-order secular resonances.

In Table 5, we show some of the actual Trojans that are at a distance smaller than 0.1 "/yr of some secular resonance related to the Great Inequality and belonging to *Family 4* (8). The computations are done up to order 24 and, even though some Trojans are found inside high order resonances, only the cases close to the largest ones (i.e. $(-1,0,0)$, $(0,-1,0)$ and $(-2,1,0)$) are

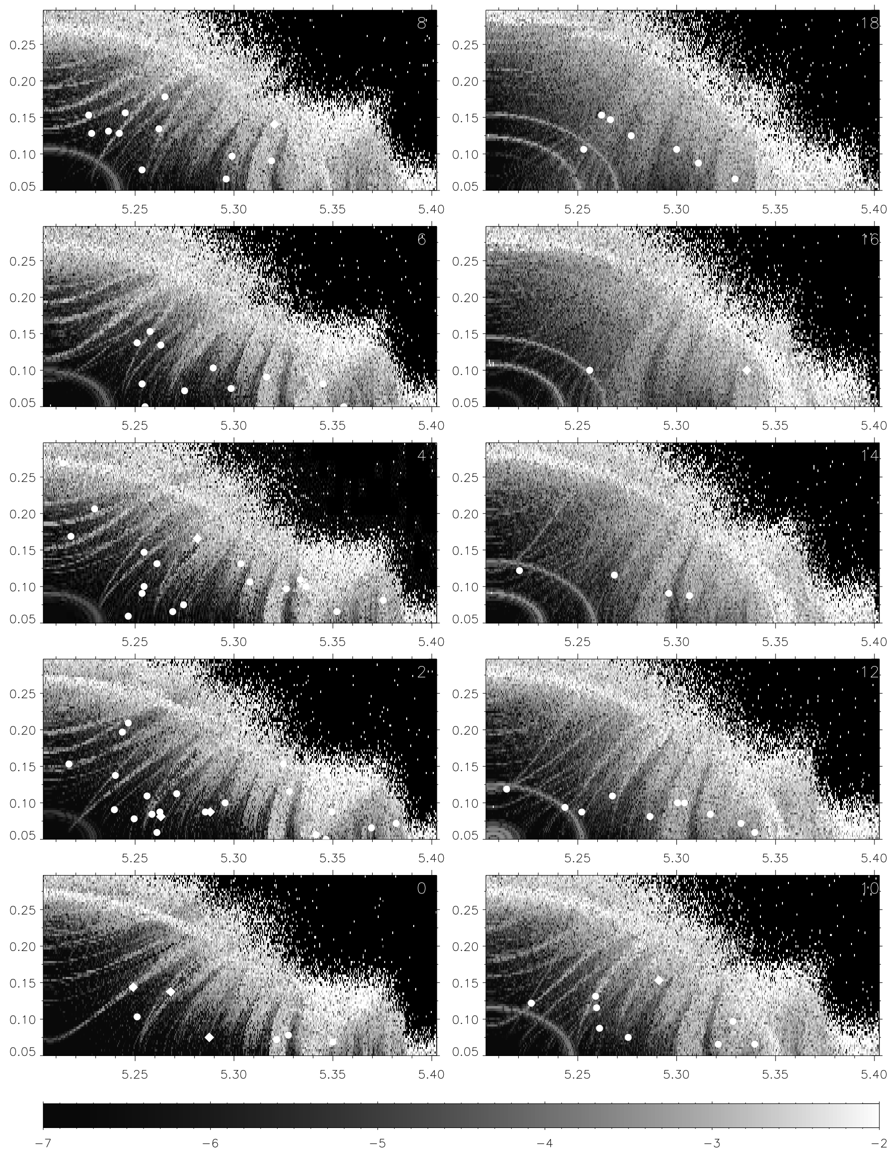

Figure 3: Dynamical maps of the tadpole region surrounding L_4 for inclinations going from I_5 (left-bottom corner) to $I_5 + 18°$ (top-right corner). The axis correspond to the semi-major axis a_0 and eccentricity e_0 of the particle. The white dots represent the "proper elements" (a^*, e^*) of the observed Trojans for which the distance $d_{j,0}$ defined by (10) is smaller than 1 "/yr. The white diamonds are associated to the Trojans satisfying the previous condition that moreover are closer than 0.1 "/yr of one of the resonances given in Tables 3–5. See text for details.

Cat. num.	Name	p	p_5	p_6	dist. ("/yr)	$I - I_5$
4035	1986WD	0	6	-8	3.30536e-03	
5023	Agapenor	-1	2	-3	1.02691e-02	
9430	Erichthonios	-2	6	-6	1.54293e-02	2°
9817	Thersander	0	5	-7	2.60215e-02	
11554	Asios	-1	-3	2	9.33537e-02	
13862	1999XT160	-1	7	-8	9.60684e-02	
15536	2000AG191	-2	4	-4	3.51934e-02	
24426	2000CR12	-1	-3	2	8.88632e-03	
24508	2001BL26	-2	6	-6	2.07783e-02	0°

Table 3: Family 2. Actual Trojans at a distance smaller than 0.1"/yr of the resonance $5\nu - 2(n_5 - 2n_6) + pg + p_5g_5 + p_6g_6 = 0$.

Cat. num.	Name	q	q_6	p_5	p_6	dist. ("/yr)	$I - I_5$
1173	Anchises	-5	3	4	-2	9.21333e-02	8°
3391	Sinon	2	-2	1	-1	6.58920e-02	
3451	Mentor	-6	4	2	0	9.94339e-02	
4138	Kalchas	-5	1	6	-2	8.14236e-02	2°
5023	Agapenor	3	-3	2	-2	3.22054e-02	
5126	Achaemenides	-2	-2	7	-3	6.49629e-02	
5130	Ilioneus	-6	4	2	0	6.09600e-02	
7119	Hiera	2	-2	1	-1	6.04987e-02	
7119	Hiera	-7	5	1	1	2.40070e-02	
9818	Eurymachos	1	-3	5	-3	3.38956e-02	

Table 4: Family 3. Some examples of actual Trojans at a distance smaller than 0.1"/yr of the resonance $qs + q_6s_6 + p_5g_5 + p_6g_6 = 0$, up to order 14. In this case, we only show 10 of the 46 Trojans found inside this type of resonances.

Cat. num.	Name	q_5	p_5	p_6	dist. ("/yr)	$I - I_5$
4057	Demophon	-1	0	0	1.91160e-03	
4543	Phoinix	-2	1	0	6.37993e-02	16°
5233	1988RL10	-1	0	0	2.73850e-04	
5638	Deikoon	-2	1	0	2.98601e-02	10°
5907	1989TU5	-1	0	0	3.46164e-04	0°
13184	Augeias	0	-1	0	1.31297e-02	
13790	1998UF31	-2	1	0	2.45299e-02	
14518	1996RZ30	-2	1	0	2.58076e-02	
17423	1988SK2	-2	1	0	7.00885e-05	0°
18228	Hyperenor	-1	0	0	1.99257e-03	4°

Table 5: Family 4. Actual Trojans at a distance smaller than 0.1"/yr of the resonance $4g + (2n_5 - 5n_6) + q_5 g_5 + q_6 g_6 + r_6 s_6 = 0$, for the cases $(-1, 0, 0)$, $(0, -1, 0)$ and $(-2, 1, 0)$.

shown. Note that some actual asteroids (for instance, 4057–Demophon, 5233–1988RL10, 5907–1989TU5, 17423–1988SK2 and 18228–Hyperenor) are really very close (distance $< 2 \times 10^{-3}$ "/yr) to one of these resonances. Actually, in some cases, it can be numerically shown that these particles are captured by these resonances and the period of libration of the critical angle inside the resonance is about several million years [26].

Finally, let us note that we have found some remarkable examples that are present at the same time in one of the tables of resonances and in the global dynamical maps of Figure 3 (they are marked with a non-blank last column in Tables 3–5). More concretely, in the 0° inclination picture we can identify 24508–2001BL26 (Table 3), and 5907–1989TU5 and 17423–1988SK2 (Table 5); at 2°, 9430–Erichthonios (Table 3) and 4138–Kalchas (Table 4); at 4°, 18228–Hyperenor (Table 5); at 8°, 1173–Anchises (Table 4); at 10°, 5638–Deikoon (Table 5) and at 16°, 4543–Phoinix (Table 5).

Some of these bodies are inside unstable structures associated to one of the families described above. These are examples of "stable chaos" [22]. For instance, 4543–Phoinix is in stable chaos according to [20] and we can locate it in Figure 3 (16° case) inside one of the secular resonances.

Moreover, the three asteroids inside the resonance $4g + (2n_5 - 5n_6) - 2g_5 + g_6 = 0$ that appear in Figure 3 (17423–1988SK2 (0°), 5638–Deikoon (10°) and 4543–Phoinix (16°)) show the displacement of this resonance in function of the initial inclination. This resonance exits the region of stability when the inclination increases. Also, the resonance $4g + (2n_5 - 5n_6) - g_5 = 0$ follows the same evolution. Two examples of asteroids inside this latter case are: 5907–1989TU5 (0°) and 18228–Hyperenor (4°).

A last interesting example that we want to point out is 1173–Anchises (Table 4 and Figure 3 (8°)). This asteroid lies inside a region of overlapping and it was already in the list of "stable chaos" in [23]. It is very close to the $s = s_6$ resonance, to a resonance of *Family 2* with $p = -2$ (6) and to a secular resonance.

4 Conclusions

In this paper, we have performed a systematic study of the global dynamical structure of the Sun-Jupiter triangular regions in the SJS model. Moreover, we have identified and classified in four families the main resonances that form the dynamical skeleton and dictate the long-term dynamics of the Trojan asteroids. In addition, we have shown how to place the actual Trojans in the global dynamical maps in a consistent way and we have been able to associate some of them with particular resonances of the four main families.

The method outlined in this paper seems to be very promising in order to study a particular real asteroid in its dynamical environment. Moreover, once the dynamical maps are computed, it is easy to add new observed Trojans and, if necessary, easy to increase the number of points of the domain $\tilde{\mathcal{F}}$ (see Section 3) to get a better accuracy of the asteroids locations.

On the other hand, inside regular regions, it is also possible to improve the determination of (a^*, e^*, I^*) (Section 3) by using interpolation of the n $(n > 1)$ closest points satisfying (10).

Finally, we cannot end the paper without mentioning that to have really accurate results for the observed Trojans, one should take into account the effect of the four major planets (OSS model). This is planned as future work.

Acknowledgements

We thank the comments of K. Tsiganis on a preliminary version of this paper. A financial support from the PNP-CNRS is acknowledged. F.G. and A.J. have been supported by the MCyT/FEDER Grant BFM2003-07521-C02-01, the CIRIT grant 2001SGR–70 and DURSI. The IBM-SP4 at CINES and Hidra at DSG-UB computing clusters have been widely used.

References

[1] C. Beaugé and F. Roig. A semianalytical model for the motion of the trojan asteroids: Proper elements and families. *Icarus*, 153:391–415, 2001.

[2] R. Bien and J. Schubart. Trojan orbits in secular resonances. *Celestial Mech.*, 34:425–434, 1984.

[3] E. Bowell. The asteroid orbital elements database, 2001. For more information, visit the URL `http://www.naic.edu/~nolan/astorb.html`.

[4] A. Celletti and A. Giorgilli. On the stability of the Lagrangian points in the spatial Restricted Three Body Problem. *Celestial Mech.*, 50(1):31–58, 1991.

[5] R. Dvorak and K. Tsiganis. Why do Trojan ASCs (not) Escape? *Celestial Mech.*, 78:125–136, 2000.

[6] S. Ferraz-Mello. A symplectic mapping approach to the study of the stochasticity in asteroidal resonances. *Celestial Mech.*, 65:421–437, 1997.

[7] F. Gabern. *On the dynamics of the Trojan asteroids.* PhD thesis, Univ. Barcelona, 2003. `http://www.maia.ub.es/~gabern/`.

[8] F. Gabern and À. Jorba. A restricted four-body model for the dynamics near the Lagrangian points of the Sun-Jupiter system. *Discrete Contin. Dynam. Systems - Series B*, 1(2):143–182, 2001.

[9] F. Gabern and À. Jorba. Generalizing the Restricted Three-Body Problem. the Bianular and Tricircular coherent problems. *Astron. Astrophys.*, 420:751–762, 2004.

[10] F. Gabern, À. Jorba, and P. Robutel. On the accuracy of Restricted Three-Body Models for the Trojan motion. *Discrete Contin. Dynam. Systems*, 11(4):843–854, 2004.

[11] A. Giorgilli, A. Delshams, E. Fontich, L. Galgani, and C. Simó. Effective stability for a Hamiltonian system near an elliptic equilibrium point, with an application to the restricted three body problem. *J. Differential Equations*, 77:167–198, 1989.

[12] A. Giorgilli and C. Skokos. On the stability of the Trojan asteroids. *Astron. Astrophys.*, 317:254–261, 1997.

[13] À. Jorba and J. Villanueva. On the persistence of lower dimensional invariant tori under quasi-periodic perturbations. *J. Nonlinear Sci.*, 7:427–473, 1997.

[14] J. Laskar. The chaotic motion of the Solar System. A numerical estimate of the size of the chaotic zone. *Icarus*, 88:266–291, 1990.

[15] J. Laskar. Introduction to frequency map analysis. In C. Simó, editor, *Hamiltonian Systems with Three or More Degrees of Freedom*, NATO ASI, pages 134–150. Kluwer, Dordrecht, 1999.

[16] J. Laskar and P. Robutel. High order symplectic integrators for perturbed Hamiltonian systems. *Celestial Mech.*, 80:39–62, 2001.

[17] H.F. Levison, E.M. Shoemaker, and C.S. Shoemaker. The long-term dynamical stability of Jupiter's Trojan asteroids. *Nature*, 385:42–44, 1997.

[18] F. Marzari and H. Scholl. On the Instability of Jupiter's Trojans. *Icarus*, 159:328–338, 2002.

[19] T. Michtchenko, C. Beaugé, and F. Roig. Planetary migration and the effects of mean motion resonances on jupiter's trojan asteroids. *Astron. J.*, 122:3485–3491, 2001.

[20] A. Milani. The Trojan asteroid belt: proper elements, stability, chaos and families. *Celestial Mech.*, 57:59–94, 1993.

[21] A. Milani. The dynamics of the trojan asteroids. In *IAU Symp. 160: Asteroids, Comets, Meteors 1993*, volume 160, pages 159–174, 1994.

[22] A. Milani and A. M. Nobili. An example of stable chaos in the solar system. *Nature*, 357:569–571, June 1992.

[23] A. Milani, A. M. Nobili, and Z. Knezevic. Stable chaos in the asteroid belt. *Icarus*, 125:13–31, January 1997.

[24] D. Nesvorny and L. Dones. How long-live are the hypothetical trojan populations of saturn, uranus, and neptune? *Icarus*, 160:271–288, 2002.

[25] D. Nesvorny, F. Thomas, S. Ferraz-Mello, and A. Morbidelli. A perturbative treatment of the co-orbital motion. *Celestial Mech.*, 82:323–361, 2002.

[26] P. Robutel, F. Gabern, and A. Jorba. The resonant structure of the Jupiter's Trojan asteroids and its evolution. In preparation, 2004.

[27] P. Robutel and J. Laskar. Global dynamics in the solar system. In H. Pretka-Ziomek, E. Wnuk, P. K. Seidelmann, and D. Richardson, editors, *Dynamics of Natural and Artificial Celestial Bodies*, pages 253–258. US/European Celestial Mechanics Workshop, Kluwer Academic Publishers, 2000.

[28] P. Robutel and J. Laskar. Frequency map and global dynamics in the Solar System I. *Icarus*, 152:4–28, 2001.

[29] C. Skokos and A. Dokoumetzidis. Effective stability of the Trojan asteroids. *Astron. Astrophys.*, 367:729–736, 2000.

[30] K. Tsiganis, H. Varvoglis, and R. Dvorak. Chaotic diffusion and effective stability of jupiter trojans. Preprint, 2004.

[31] C. Yoder. Notes on the origin of the trojan asteroids. *Icarus*, 40:341–344, 1979.